City Research Online

City, University of London Institutional Repository

Citation: Jadidbonab, H., Malgarinos, I., Karathanassis, I. K. ORCID: 0000-0001-9025-2866, Mitroglou, N. ORCID: 0000-0002-2955-8716 and Gavaises, M. ORCID: 0000-0003-0874-8534 (2018). We-T classification of diesel fuel droplet impact regimes. Proceedings of the Royal Society A: Mathematicsl, Physical and Engineering Sciences, 474(2215), doi: 10.1098/rspa.2017.0759

This is the accepted version of the paper.

This version of the publication may differ from the final published version.

Permanent repository link: http://openaccess.city.ac.uk/20506/

Link to published version: http://dx.doi.org/10.1098/rspa.2017.0759

Copyright and reuse: City Research Online aims to make research outputs of City, University of London available to a wider audience. Copyright and Moral Rights remain with the author(s) and/or copyright holders. URLs from City Research Online may be freely distributed and linked to.

City Research Online: http://openaccess.city.ac.uk/ publications@city.ac.uk

We-T classification of Diesel fuel droplet impact regimes

Hesamaldin Jadidbonab*, Ilias Malgarinos, Ioannis Karathanassis, Nicholas Mitroglou and Manolis Gavaises
Department of Mechanical Engineering, City University of London, UK
*Corresponding author: hesamaldin.jadidbonab.1@city.ac.uk

Abstract

A combined experimental and computational investigation of micrometric Diesel droplets impacting on a heated aluminium substrate is presented. Dual view high-speed imaging has been employed to visualise the evolution of the impact process at various conditions. The parameters investigated include wall surface temperature ranging from 140 to 400 °C, impact Weber and Reynolds numbers of 19-490 and 141-827 and ambient pressure of 1 and 2 bar. Six possible post-impact regimes were identified, termed as *Stick, Splash, Partial-Rebound, Rebound, Breakup-Rebound and Breakup-stick*, and plotted on the *We-T* map. Additionally, the temporal variation of the apparent dynamic contact angle and spreading factor have been determined as a function of the impact Weber number and surface temperature. Numerical simulations have also been performed using a two-phase flow model with interface capturing, phase-change and variable physical properties. Increased surface temperature resulted to increased maximum spreading diameter and induced quicker and stronger recoiling behaviour, mostly attributed to the change of liquid viscosity.

Keywords: Diesel, droplet, hot surface, Leidenfrost, impingement, CFD

1 Introduction

Understanding liquid droplet impact onto solid surfaces is important in a number of industrial applications such as IC engines, fire suppression, thermal power plants, microprocessor cooling, and ink printing among others. Due to the fact that the aforementioned spray systems may be comprised of millions of interacting droplets that prohibit detailed identification of the flow conditions during the impact of individual droplets, many studies focus on the characterisation of the impact dynamics of single droplets under well-controlled conditions. Several parameters, such as droplet velocity, diameter and angle of impact [1], liquid physical properties [2], surface conditions [3], wall surface temperature (T_w) [4] and ambient pressure [5] are of key importance for the deformation of droplets upon impact and thus, define the impact outcome. These parameters define the Reynolds ($Re=\rho V_0 D_0/\mu$), Weber ($We=\rho V_0^2 D_0/\sigma$) and Ohnesorge ($Oh=\sqrt{We}/Re$) dimensionless numbers that are frequently utilised to macroscopically characterise the process (where ρ is the liquid droplet density, σ the liquid vapour surface tension, μ the viscosity, D_0 the initial droplet diameter and V_0 the impact velocity). Comprehensive reviews of recent advancements in this area, from the flow dynamic point of view, can be found in [6], [7].In general, the post-impact outcome regimes can be illustrated on regime maps as a function of surface temperature and impact Weber number, as reported in [4], [8]–[10] for various single component liquids. In [10], the impact outcomes are defined by means of hydrodynamic regimes and droplet morphology (stick, splash, break-up and rebound), while in the rest, more attention is given to the heat transfer associated with the corresponding boiling modes; the regimes identified include film evaporation for $T_W<T_{BP}$, nucleate boiling for $T_{BP}<T_W<T_L$ and film boiling for $T_W>T_L$. Moreover, upon impacting on a heated surface with temperature much higher than liquid's boiling temperature, a thin layer of the droplet own vapour forms between the solid surface and the droplet, that is typically only a few nanometres thick [4]; this layer may prevent the contact between liquid and solid which, in turn, decreases the heat transfer rate. If the pressure force exerted on the droplet from the vapour layer overcomes the droplet's weight, then it levitates from the surface and may rebound; this is known as the Leidenfrost regime[11]. Recently, relying on high-speed imaging techniques, different influential aspects of this transition temperature i.e. fingering patterns, vapour layer thickness and residence time have been reported in [12]–[14]. In [15] it was reported that the dynamic Leidenfrost temperature is influenced by the droplet size. Furthermore, the investigations of [16] have reported a variable Leidenfrost temperature according to droplet impact velocity. Increasing the surface roughness is also reported to increase the Leidenfrost temperature [17]; however this temperature decreases by decreasing the impact angle. It can be also expected that an increase in the ambient pressure and air density at a given temperature, increases the Leidenfrost temperature, due to the change in liquid's boiling point [18] and the difference in aerodynamic and buoyancy forces.

In addition to the characterisation of the post-impact outcome, quantification of the droplet's spreading rate and wetting behaviour are often studied. Understanding of the spreading behaviour is essential for the determination of the wetting dynamics and thus the impact outcome. In [19], the dynamic contact angle and spreading factor have been employed extensively to study droplet dynamic wetting behaviour onto solid substrates. The value of contact angle, which changes

during droplet spreading, can be measured from images of the droplet's profile at the moving contact line. The flow at the contact line determines the value of dynamic contact angle and thus, contributes to spreading rate [20]. Several experimental studies have been carried out recently to measure the temporal variation of contact angle and the spreading factor under isothermal condition (selectively [21], [22] among many other). Nonetheless, the phenomena of non-isothermal droplet impact are more complex, due to added influential factors related to heat transfer process, evaporation, and temperature dependence of the liquid physical properties. When $T_W<T_{BP}$, the heat transfer does not affect the phenomenon at the beginning of the droplet impact process [23]. However, later on during spreading, the temperature rise inside the droplet alters the evaporation process and the physical properties of the droplet (i.e. surface tension and viscosity); this may result in modification of the spreading rate. In [24] the equilibrium and dynamic advancing and receding contact angles of water droplet impacting on copper and stainless steel surfaces at wall temperatures ranged from 120-200 °C, were reported. They observed significant change in dynamic receding contact angle with respect to surface temperature and noted this effect as an indicative parameter of change in boiling regime. It is suggested by [25] that the rapid evaporation at the edges of the spreading droplet causes it to curl back and increase the dynamic contact angle. In [26] the spreading dynamic of a water droplet on a heated hydrophilic and hydrophobic textured surfaces have been examined and a strong influence of surface temperature on droplet spreading factor for the hydrophilic surfaces has been observed.

The majority of the previous experimental studies have employed water droplet with a wide range of diameters (several hundred micrometres to several millimetres) [27], [28]. In addition, glycerine/water mixture [29]–[31], alcohols [32], silicon oil [33]–[35], aqueous polymer solution [36], [37], single component hydrocarbons [38], [39], FC-72 [40]–[42] and non-Newtonian fluids [43] have also been used to investigate the impinging droplet phenomena. In [38] the impact behaviour of a binary fuel droplet onto a heated copper plate has been studied; the fuel droplet consisted of a mixture of n-hexane and n-decane, which have significantly different boiling temperatures. They have shown that the impact regimes obtained from their fuel mixture are significantly different from the regimes of a single component fuel, in particular when wall surface temperature was above the n-hexane boiling temperature. In [44] the evaporation lifetime curve of a binary fuel droplet on a heated surface has been studies; two local maximum and minimum vaporisation rates (as a function of surface temperature) have been observed while for a single component case there is only one local maximum and one local minimum.

The review of the literature given above indicates that despite the information available characterizing the isothermal and non-isothermal droplet impact onto flat surfaces, only limited information exists regarding hydrodynamic (inertia, capillary and viscous forces) and thermal (heat flux) effects for Diesel fuel droplet impact on flat heated surfaces [45]. It should be noted that a complete impact outcome map for a wider range of Weber numbers and wall surface temperatures for Diesel droplets has not yet been presented. This paper aims to bridge this gap by reporting new experimental data of micrometric Diesel fuel droplet impingement on a heated aluminium surface. The post-impact regimes are identified and mapped for a wide range of Weber-T set points, by means of high-speed imaging. The temporal variation of dynamic contact angle and spreading is derived for conditions below the Leidenfrost point for which no splashing/breakup occurs. In addition, conditions leading to the onset of droplet splashing/break-up are studied and the effects of substrate temperature, *We* number and air density on the disintegration process are identified. In addition to experiments, CFD simulations assist in the interpretation of the observed droplet behaviour are reported together.

2 Materials and methods

2.1 Experimental Setup

A schematic of the experimental setup is depicted in Figure 1. It consists of a constant volume chamber with three quartz windows providing undisturbed optical access, a mono-droplet dispenser, a heated aluminium surface, two high-speed cameras, and the data acquisition system.

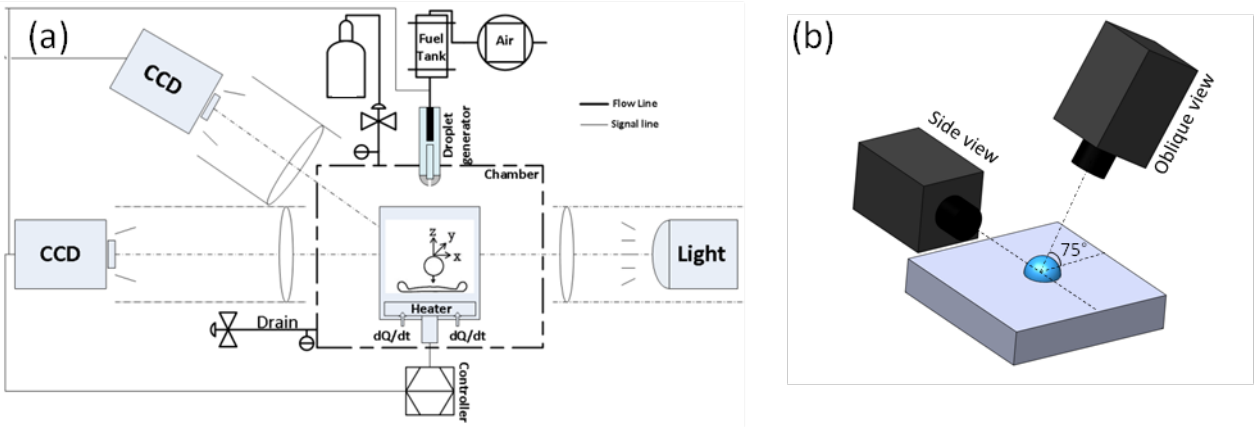

Figure 1: (a) Schematic illustration of the test rig set-up utilised (b) 3D positioning of the cameras

An aluminium specimen, with dimensions of 50x50x20 mm, was used as the target solid surface; it was grinded to a ground finish with an average surface roughness of R_a=0.8 µm and was subsequently polished using a 1µm diamond paste to reduce the surface roughness to R_a=0.4±0.01µm. The surface roughness was measured using a linear surf-metre (Mitutoyo Surftest-SJ-500). The specimen was heated by three 250W cartridge heaters (type HLP, TURK HILLINGER), embedded 3mm under the target surface and allowing a maximum temperature of 400°C to be achieved. This covers the entire range of boiling modes, from nucleate up to above the Leidenfrost temperature. Experiments for each individual impact scenario were conducted once steady-state temperature of the wall was reached. Temperature measurements were taken by three K-type thermocouples with an accuracy of ±1.5°C for the largest recorded temperature value. These thermocouples were integrated into the specimen, next to the heaters. A closed chamber with optical access was utilised to control the air pressure. Three additional thermocouples were used to monitor the ambient temperature of the chamber at different locations. The injected droplet temperature was kept at 25±1°C by means of a water heat exchanger and a layer of insulation mounted on the droplet generator system to avoid external heating of the fuel liquid from the heater.

The liquid used in this study was standard summer Diesel fuel with properties ρ=833 kg/m3, σ=28.9 mN/m and μ=2.7 cP at 25°C. Due to the heat transfer from heated wall surface to the droplet, the temperature and properties of the droplet, during the impact period, change. In order to ensure a fuel vapour-free atmosphere within the test chamber, the chamber was evacuated after each impact and fresh gas was purged into the chamber prior to each experiment. Mono-droplets were generated from a delicate electromagnetic dispensing system (SLMD300G, Fritz Gyger AG). The droplet injection process was controlled with compressed air and precise opening time of the injector anchor; the measured droplet size and velocity were in the range of 320-440µm and 1.4-6.18m/s, respectively. These correspond to impact Weber and Reynolds numbers in the range of 19-490 and 141-827, respectively. A full description of the operating conditions investigated is listed in Table 1.

Case No.	D_0 [µm]	u_0 [m/s]	We [-]	Re [-]	Surface temperature [°C]
1	320	1.42	19	141	
2	370	2.41	65	280	
3	410	4.15	202	510	$140 < T_W < 400$
4	440	5.25	360	710	
5	440	6.18	490	827	

Table 1: Table of conditions tested

Two synchronised Photron high-speed cameras (Photron SA1.1 and APX-RS), providing 12-bit greyscale images at a rate of 30k fps, were used to visualise the droplet impact process with 640x288 and 256x256 pixel resolution for the side and the oblique views, respectively. The quantitative measurements were made using the side view images. The

high magnification optical system consisted of a long distance (LD) microscopic lens (infinity DistaMax) and a 12x zoom lens (Thorlab); the resolutions obtained were 3.78±0.02 and 5.6±0.4μm/pixel for the side and oblique views, respectively. The back to front illumination was provided using two 250W ARRI metal halide continuous white light sources. The best compromise between the image brightness and the edge sharpness was achieved by setting the exposure time to 2.1 and 4μs for side and oblique view, respectively. The droplet displacement of largest velocity during this time interval is less than one pixel, resulting in ±3.78μm uncertainty in droplet edge position. In total, with respect to droplet impact Weber number and wall surface temperature, 130 conditions were tested.

Image processing was performed using an in-house MATLAB routine to determine the pre-impact parameters (D_0, V_0) and spreading parameters (θ, β). Starting from the raw images and using the edge detection algorithm reported in [46], the extraction of the droplet profile at two different time steps is obtained. This method is based on the pixel intensity gradient, determining the position and orientation of the edge within each individual pixel. More specifically, initially, a threshold is specified by comparing the mean pixel intensity of the regions inside and outside of the droplet. The horizontal and vertical positions of the edge points are then registered in Cartesian coordinates. A cubic polynomial fitting curve is derived through the first 10 adjacent points on both the left and right corners near the triple contact point and at each time instant. The coefficients of determination (R^2) of the fitting curves were above 99% for all the test cases. The apparent dynamic contact angle $\theta_D(t)$ was measured from the tangent line drawn on the fitted polynomial at the triple contact point, with an accuracy of ±2°. To establish repeatability of the measurements, each test case was repeated up to 5 times; as the observed maximum variation was less than 2% in dynamic contact angle and spreading factor, only the mean value of each parameter is reported here. The spreading diameter D(t) was computed as the distance between right and left triple contact points, with a maximum uncertainty of ±8μm; these values were then non-dimensionalised using the pre-impact droplet diameter D_0 and denoted as β (spreading factor). The standard deviation of measured spreading factor and non-dimensionless height in each case was less than 2.5%. The pre-impact conditions were also obtained from the acquired droplet image immediately before the impact. The droplet was not perfectly spherical, so both vertical and horizontal diameters of the ellipsoidal image of ovoid droplet were considered, and the equivalent diameter was estimated, as in [47], according to:

$$Deq = (D_v D_h^2)^{1/3} \quad \textbf{(1)}$$

Where D_v and D_h are the vertical and horizontal dimension, respectively, assuming the droplet is rotationally symmetric with respect to the vertical axis. The vertical and horizontal diameters differed by less than 1.5% for We=19 and 5% for We=490. The mean equivalent diameter in each test case was calculated with standard deviation of 2.5%. The impact velocity was derived from the centroid values in two consecutive images of the droplet immediately before impact with an accuracy of 0.07m/s at We=19 and 0.11m/s for We=490. The relative uncertainty in the calculated Weber number ranged from ±0.7 at We=19 and to ±8 at We=490.

2.2 Numerical Methodology

The use of a Computational Fluid Dynamics model, as developed recently by the authors [48]–[50] has been also employed in order to assist in the interpretation of the recorded images. This model has been validated for numerous cases of droplet impingement onto flat and spherical surfaces, with and without heat transfer. The CFD model solves the Navier-Stokes equations for mass and momentum conservation, while it employs the VOF methodology to capture the liquid-gas interface. The energy equation coupled with a species transport equation for the vapour and a local evaporation model are utilized to simulate phase change [49]. The evaporation rate is based on the kinetic theory of gases, where the driving force is the difference between the saturation conditions at the interface and the conditions on the vapour side. This model has been validated in [49] for single droplet evaporation and impingement for an n-heptane droplet. In this work it is utilized for the simulation of Diesel drop evaporation and validated against the experimental data of [51], [52] for Diesel. A dynamic local grid refinement technique was used to keep the computational cost at affordable levels [53]. In Figure 2, the axisymmetric domain used in the current study is presented, along with a zoomed region that shows the application of the dynamic grid refinement technique at the liquid-gas interface at the time instant of maximum spreading. The numerical model is used to predict the spreading dynamics for stick and breakup regimes. To capture rebound, the grid should be massively refined next to the wall surface [54] in order to resolve the thin vapour layer formed.

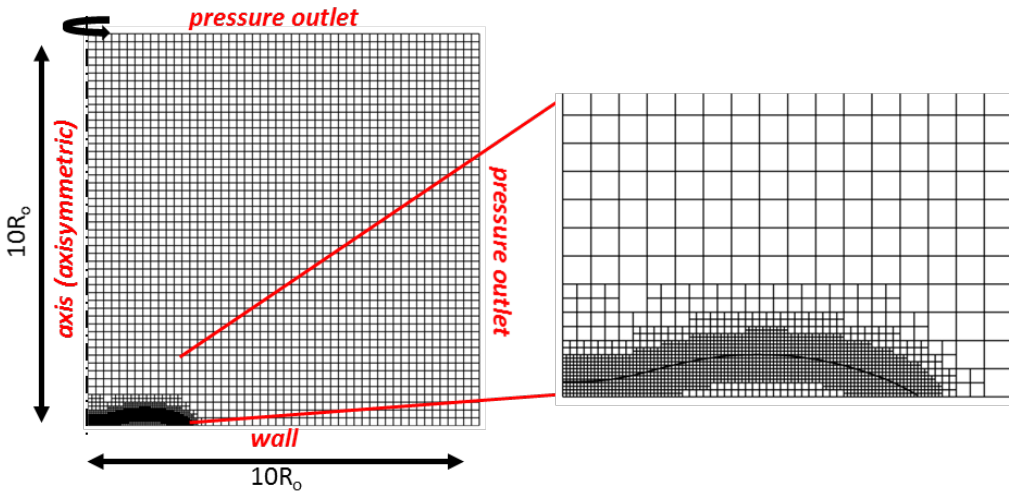

Figure 2: (a) 2D-axisymmetric computational domain and boundary conditions used for the simulation of Diesel droplet impingement, (b) grid refinement of the liquid-gas interface

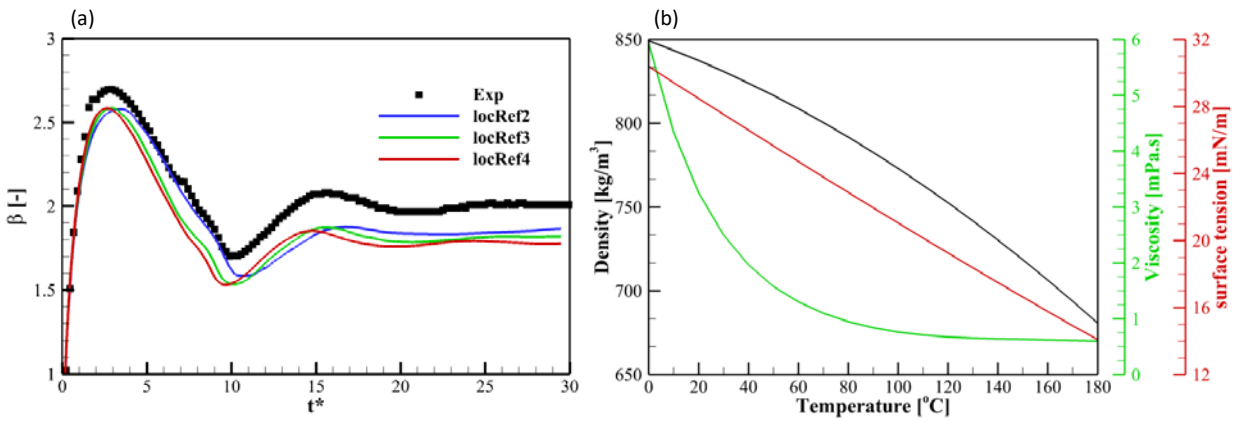

Figure 3: (a) Grid dependency study: Temporal evolution of the spreading factor β for the case of T_W=140°C, We=65. (b) Temperature dependence properties of Diesel fuel [55]

The boundary conditions, also depicted in Figure 2, include symmetry (axisymmetric domain), pressure outlet in the open (free stream) boundaries and no-slip wall condition. A constant temperature value is applied at the wall boundary. The base initial grid consists of 50x50 rectangular cells. After the application of three levels of local refinement, the droplet radius is resolved by 40 grid cells. In Figure 3a, a grid independency study is presented for the case of T_W=140°C, We=65; the non-dimensional time t* has been defined as $t^* = (t x V_0)/D_0$, where, t=0 is the time at the instant of impact, while V_0 and D_0 are the initial droplet velocity and diameter, respectively. It is clear that increasing the levels of refinement from 3 or above, the numerical predictions converge to a similar distribution for the temporal evolution of the spreading factor β.

The dynamic contact angle model of Kistler was utilised as implemented in [53], using the equilibrium contact angle value of 23 degrees; this was measured at the end of relaxation phase under room temperature conditions. Although the direct imposition of the dynamic contact angle temporal evolution, as taken from experiments can be applied, it is not used in this study, as the basic aim of the simulations is to exhibit the effect of surface temperature on the spreading/recoiling dynamics. The change in liquid properties as the temperature increases, affects the contact angle variation, especially during the droplet recoiling phase, as it is shown in the following section; direct imposition of the measured contact angle variation would prevent the prediction of this behaviour. Figure 3b depicts the temperature dependent properties of the Diesel liquid for a temperature range of 0-180°C i.e. up to its boiling point at 1bar pressure.

All properties are taken from [56], except for the vapour pressure which is over predicted; the corresponding values for n-tetradecane are used instead [57]. The properties of this compound behave similarly to Diesel, as mentioned in [58].

3 Results and Discussion

3.1 Classification of post–impact regimes

In general, under the operating conditions defined in Table 1, essentially six different macroscopic outcome regimes have been identified, termed as: stick, splash, rebound, partial-rebound, breakup and breakup-rebound as illustrated in Figure 4. The droplet impact process and outcome regime depends on Weber number as well as the target surface temperature.

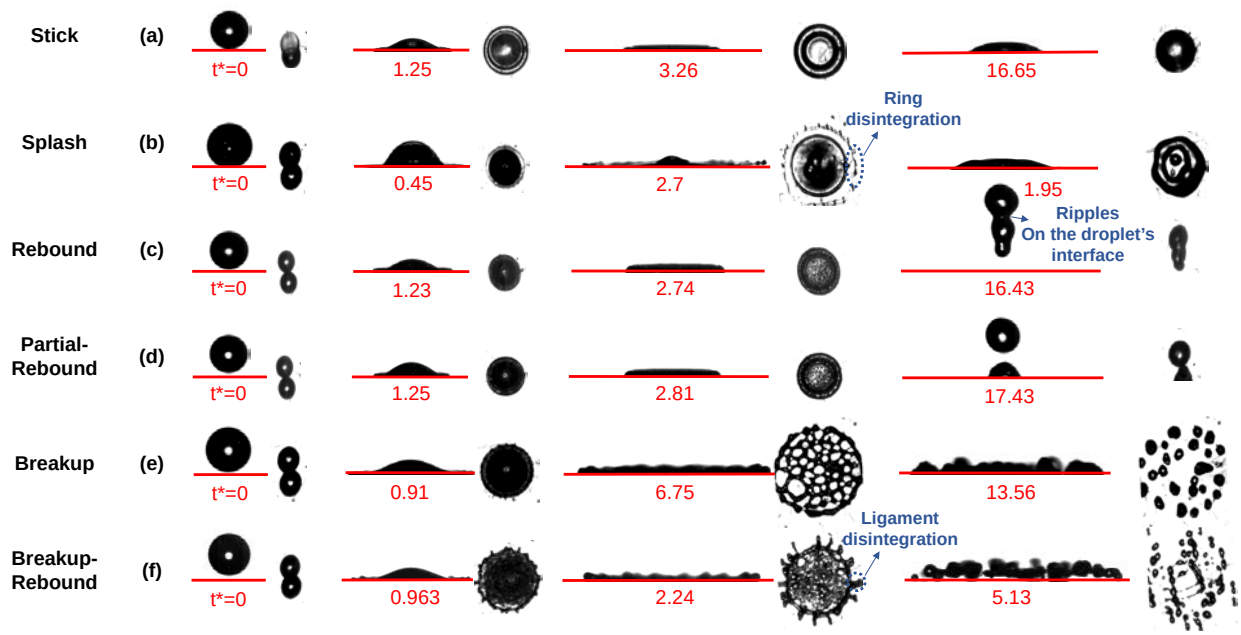

Figure 4: Temporal evolution of Diesel fuel droplet during impact on the heated flat aluminium surface for different values of Weber number and wall temperature; (a) stick regime at We=65, T_W=170°C; (b) splash regime at We=490, T_W=180°C; (c) rebound regime at We=65, T_W=350°C; (d) partial rebound regime at We=65, T_W=340°C; (e) breakup at We=490, T_W=340°C; (f) breakup-rebound regime at We=202, T_W=370°C

In the "stick" regime (Figure 4a), the entire mass of the droplet is deposited on the wall surface upon impact (t*=1.25), spreads (t*=3.26) and finally relaxes on the surface (t*=16.55). The initial kinetic energy of the droplet is lost into viscous dissipation during spreading. This regime occurs for Weber numbers below the splash threshold and/or when the heat transfer is not intense enough to induce breakup or rebound. Increased heat transfer induces boiling within the bulk of the liquid, which has been identified as one of the droplet disintegration mechanisms [59]. "Splash" (Figure 4b) occurs when We is high enough so the droplet becomes unstable (t*=0.45), deforms and forms smaller droplets after the disintegration of the moving edge of the spreading lamella (t*=2.7); however, the rest of the droplet stays on the surface. Two different types of disintegration patterns were observed, in the form of liquid ligaments (Figure 4f at t*=2.24) and rings (Figure 4b at t*=2.7), resulting in different splash regimes. The first one is ought to instabilities developing on the liquid film forming radially outwards. As the forming ligaments grow in length, their shape becomes unstable and eventually break up into smaller droplets. The second one is attributed to instabilities developing in the circumferential direction; as the lamella diameter increases, its thickness reduces until the formed ring at the edge of the lamella detaches and continues to expand until breaking up into smaller droplets. Similar mechanisms have been reported in [45] for both a heavy multi-component and a single component hydrocarbon fuel droplet. In the "rebound" regime (Figure 4c), the droplet impacts onto the surface (t*=0), spreads (t*=1.23), recoils (t*=2.74) and finally rebounds (t*=16.43) from the surface. A vapour cushion forms between the droplet and the heated surface (t*=1.23). In this regime there is almost no direct contact between the wall surface and the liquid droplet [4]. In the partial rebound regime (Figure 4d), capillary waves are generated in the form of ripples on the droplet's interface (65) due to the difference of the initial apparent

(near to 180°) and the static contact angle; these propagate along the liquid surface, causing the droplet to pinch off. A part of the droplet stays on the surface and the other part rebounds (t*=17.43). If the impact energy is high enough to generate a strong perturbation, then the droplet breaks into several smaller droplets (Figure 4e-f); these smaller droplets either stay in contact with the surface (breakup-stick) or rebound from it (breakup-rebound).

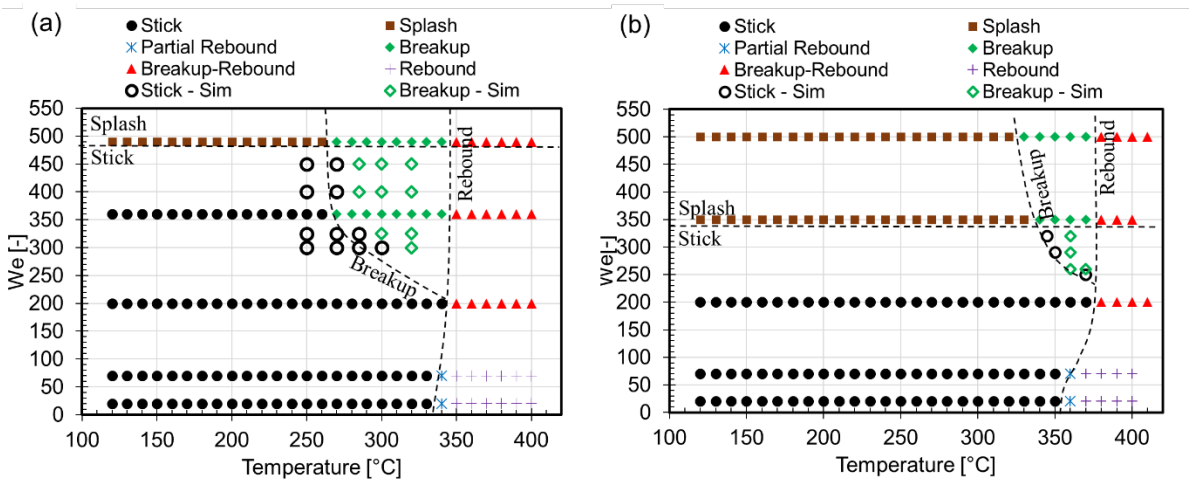

Figure 5: We-T regime diagram of Diesel fuel droplet impact on a heated aluminium surface at (a) P=1bar and (b) P=2bar Empty markers show numerical results of the transition area of breakup regime have been added.

The various post-impact outcomes as identified above have been plotted on the Weber number and wall-surface temperature diagram and shown on Figure 6 for the two different air pressures tested. The transition boundaries (dashed lines) show where a change in the droplet impingement behaviour has been observed. It should be noted that the transition lines between neighbouring regimes were not clearly determined due to the experimental uncertainties affecting the actual We-T threshold.

At 1 bar air pressure, for temperatures below the Leidenfrost point (T_L) and relatively low Weber numbers, the droplet moves laterally in contact with the heated surface until it reaches its maximum spreading. Then it recoils and relaxes into a spherical cap shape, which can be described by the apparent dynamic contact angle and spreading factor. The splash regime was observed for We>490. With regards to the droplet levitation/rebound (Figure 5c at t*=16.43), T_L was observed around 340°C for low Weber number(We≤65) and increased about 10°C for We>65; this shows the dependency of the Leidenfrost regime on the impact Weber number. The breakup regime was observed for We≥360 and 270°C<T<T_L, however the minimum temperature of breakup regime decreases 10°C for larger Weber number (We≥490). In this regime, the droplet breaks up during the retraction phase (Figure 4e at t*=6.75). High impact Weber number results in larger surface contact area and therefore a thinner liquid film is forming over the surface; this increases the overall heat transfer to the droplet mass and reduces the surface tension ability to retain the droplet shape. Thus, the liquid film ruptures and hence the droplet breaks up into smaller droplets (Figure 4e). For wall surface temperatures above the Leidenfrost point, these smaller droplets rebound from the surface after breakup (breakup-rebound regime). The minimum surface temperature required for this regime to occur is constant over the entire range of Weber numbers. The extension of transition lines, coinciding at the point of (We=202, T_W=350°C), separates the stick, breakup and rebound regimes. The same We–T set points were also examined at chamber pressure of 2 bars (Figure 5b). Similar outcomes as in the1 bar air pressure case were observed although the position of the transition lines was shifted towards higher surface temperatures and lower Weber numbers. As it is expected, the breakup and rebound regimes occur at higher temperature for increased air pressure. This can be attributed to the higher Diesel components saturation point at elevated air pressure. The Leidenfrost temperature for the rebound and breakup-rebound regimes was increased by 20°C and 30°C, respectively, compared to the 1 bar case. The transition line of breakup regime was shifted by nearly 70°C. It is already well established by previous experimental studies [5] that the gas flow in the vicinity of the moving edge is crucial for the splash development; the splash transition line, which is independent of the surface temperature, was shifted from We=490 to We=350 by increasing the ambient air pressure from 1 to 2 bars.

CFD simulations were utilised to predict the transition line for both 1 and 2 bar pressure conditions, as shown in Figure 5a and b, respectively. For Weber numbers in the range 202-360, the dominant mechanism that induces breakup is evaporation. As the solid surface temperature increases, evaporation intensifies and results gradually to breakup. For the range of surface temperatures simulated (250-325°C), the average droplet temperature at maximum spreading reaches around 55-65°C while at t*=10, rises up to 95-125°C; this shows that the rate of droplet heating increases for higher surface temperatures. At that moment, the droplet has lost a small portion (0.2-0.5%) of its initial mass. This might not seem as a significant amount; however, as the droplet heating rate increases, evaporation becomes more intense and this affects the post-impact regime, which changes from stick to breakup. At 2 bar air pressure, the breakup regime is limited to a small area and an average droplet temperature of approximately 135°C at t*=10 is reached for all cases. For higher We numbers (We≥360), the impact kinetic energy becomes more dominant, as the transition line is almost vertical in respect to surface temperature. Droplet temperature at t*=10 is similar compared to the lower Weber number (202≤We≤360) cases (100-130°C), as well as the liquid mass evaporated (0.15-0.5%). The trend for the transition from stick to breakup mode, as predicted from CFD, is similar to the experimental one; the differences seen between experiments and predictions have been primarily attributed to the Diesel properties utilised and more specifically to the vapour pressure and fuel composition. As Diesel has been approximated as a single component fluid, its vaporisation process is inevitable different from the real Diesel fuel. Such hydrocarbon fuel mixtures are homogeneous as long as the temperature remains below the boiling temperature of the individual components. However, they behave differently from a single component fluid at surface temperatures higher than some of the components' boiling temperatures due to preferential vaporisation. Up to now, classification of the post impact outcome on heated surfaces has been reported in the literature only on single component liquids; thus, the existing regime maps and transition criteria available so far are not applicable for Diesel, which comprises of more than 300 components covering light to heavy hydrocarbon molecules. In order to highlight the differences in the impact outcome of the multi- and single component fluids, new experimental data for the Leidenfrost temperature, breakup, and splash have been compared to those previously reported in the literature.

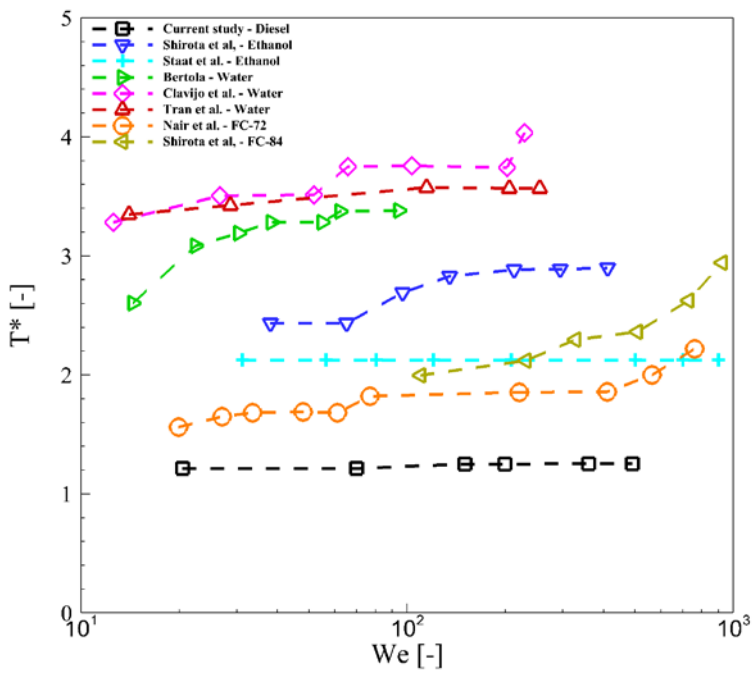

Figure 6: Transition temperature to the Leidenfrost temperature (T_L) as a function of We. The first data set is for the current study, followed by data representing Leidenfrost temperature values of ethanol impacting on a heated polished silicon [60] and a sapphire glass plate [4], respectively. The third data set is from [9] and illustrates the experimental results of a water droplet impact on a heated polished aluminium surface. The next two data sets represent the impingement of a water droplet on a heated, polished silicon wafer as reported by [61], [62]. Finally, the last two data sets are for impact of FC-72 [42] and FC-84 droplets [4] on a heated, sapphire glass plate.

In general, significant discrepancies exist in the literature with regards to the quantification of the transition between the post-impact regimes. Figure 6 shows the transition to the Leidenfrost temperature (based on the data extracted from the regime map depicted in Figure 5) as a function of impact Weber number. The Leidenfrost-temperature values of the

current study are compared against those derived by the experiments carried out by [9], [61], [62] for water, [4], [60] for ethanol and [4], [42] for fluorocarbons, and are normalised by the respective liquid's saturation temperature ($T^*=T_w/T_{BP}$) for 1bar pressure; T* can be denoted as the degree of wall superheat. It should be noted that based on the data of [56], the so-called average boiling temperature of Diesel fuel at atmospheric pressure can be assumed to be 280°C. In general, the larger the Weber number, the higher the wall-surface temperature required to initiate rebounding and consequently T_L increases [62], [63]. For instance, considering water, several different values, ranging from 150 to 310°C, for the Leidenfrost temperature have been reported in [64]–[67]. The discrepancies in the reported values arise from differences in liquid impinging mass, impact velocity, amount of liquid sub-cooling, surface roughness, solid thermal properties, ambient pressure, impurities and the degree of wall cooling under the droplet due to heat transfer. The importance of the parameter β (=1/kρc) has been observed to increase as the Weber number value increases [65], [68]. As the value of β decreases, the surface behaves isothermally and consequently, the lower value of the T_L is. This can explain the higher wall superheat ratios required for transition to Leidenfrost in case of sapphire and silicon plates compared to aluminium. In addition, the temperature dependent contact angle is believed to be an influential parameter to control the stability of the vapour layer forming between the liquid and the wall surface, affecting the transition to the Leidenfrost temperature [69]. As the contact angle decreases, the heat flux increases at the impact moment, so the required temperature of stable vapour layer decreases. In the present investigation, the high wettability of the Diesel liquid on aluminium plate, explains the lower wall superheat required for Leidenfrost transition.

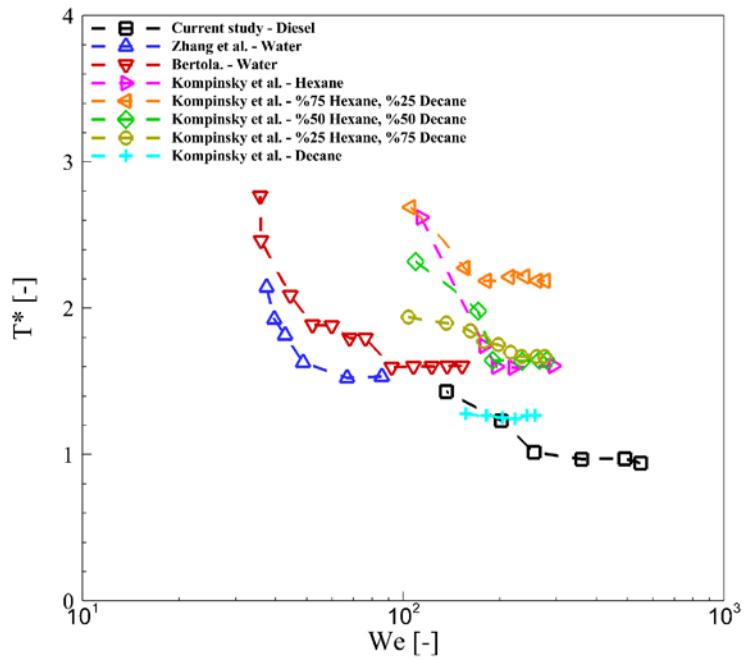

Figure 7: Critical surface temperature for droplet breakup as a function of Weber number. The first data set corresponds to the current study, followed by data obtained for the break up transition of a water droplet colliding on a heated silicon wafer [70] and an aluminium plate [9]. The additional data sets are from [38] and represent the breakup transition of droplets comprising different n-hexane/n-decane mixtures colliding on a heated copper plate.

The breakup regime was not observed as a post-impact outcome in most of the studies where silicon and sapphire were used, due to their very low surface roughness. In order for such a regime to arise, the inertial forces required to overcome the capillary pressure should be increased to values possibly outside the range of Weber and Reynolds numbers examined in the respective studies e.g. in [4], [62], [71]. Additionally, the high wettability of Diesel fuel on silicon and sapphire, as well as the low distribution of vapour-nucleation sites (e.g. cracks and crevices, roughness elements) compared to a polished aluminium surface, prevent the creation of disruptive vapour bubbles that initiate the boiling-induced disintegration of the droplet [9]. This behaviour is in contrast with past studies, where breakup has been observed with relatively lower Weber and surface temperature values; for instance, refer to [63], [17] discussing droplet collision onto heated metal surfaces. Figure 7 depicts in a comparative manner the minimum surface temperature required to initiate droplet breakup as a function of impact Weber number, for different liquids and impact surfaces. Similar to Figure 6, the wall-surface temperature values were normalised by the respective liquid's boiling temperature. The coupled effects of heat transfer between the droplet and the heated surface and the impact momentum induce

breakup. As it can be seen and also noted in [72], increasing Weber number, results in increased influence of the droplet kinetic energy, and hence, a lower surface temperature is required to initiate breakup. Similar behaviour has been seen in [69], where breakup of a n-decane droplet impinging on a heated substrate was independent from the wall surface temperature for T_W> 300°C. As it can be seen in Figure 7, the minimum wall-surface superheat ratios required for breakup for the water cases are qualitatively similar; some variations arise from their different surface properties. The lower wall superheat ratio values in the case of water droplet impact on a silicon plate obtained by [70] compared to the respective for impact on aluminium plate are not that clear to interpret. The lower thermal conductivity, which subsequently alters the local wall cooling and surface roughness of silicon plate should increase the required surface temperature and Weber number for breakup to occur when compared to aluminium. However, it should be noted that the surface temperature measurement in [9] has been corrected for the difference between the substrate holder and the substrate itself; a correction that lead to increased values of the surface temperature. Lower set points of (T*, We) are related to the Diesel fuel composition and surface properties. Even having similar impact surface, the breakup behaviour can be significantly different as the fuel composition changes, which is evident from the breakup behaviour of different mixtures of decane and hexane [38].

The threshold of splashing on a smooth, flat aluminium surface has been examined under a wide impact Weber number range for 1 and 2 bar pressures. Splashing occurs once the momentum of the droplet cannot be converted into the momentum of flow along the surface [73]. Therefore, increasing impact Weber number shifts the post-impact regimes from stick to splashing, confirming the results of previous studies [60], [74]. Moreover, The effect of air pressure on splashing, first studied by [74] has been verified to extend into higher ambient pressure conditions [5]. In this work an empirical correlation (based on experimental data) for splash threshold for a wide range impact conditions, considering the internal pressure generation during droplet impact and the opposing retentive surface tension [5], has been proposed as: $2.84(Ca_a)^{0.54}(\frac{P}{P_0})^{0.42}=1$. This correlation gives 99% accuracy against the present experimental findings for the splash threshold for both air pressure values investigated. In addition, regarding the numerical simulation of the splashing regime, only two numerical efforts have been performed up to now in order to successfully simulate this phenomenon in 3D domains [75], [76]; splashing is captured using either an initial perturbation in the velocity field, or due to small round-off errors in the pressure equation that initiate these perturbations. In a more recent paper [77], the authors manage to capture the dynamics of splashing using a grid refined at a size of 3000 equivalent cells near the contact line. The high computational effort needed make these runs unfeasible for the current study.

3.2 Dynamic behaviour of spreading in the stick regime

The effects of surface temperature and impact Weber number on spreading dynamics within the stick regime are further examined in this section. Figure 9 shows the sequential images of the droplet impact evolution during the spreading and receding phases for different values of the surface temperature and impact Weber number of 65. Numerical simulations are presented as well, in order to elucidate the fluid flow induced by the droplet impact. A section view at the droplet middle plane is presented in the simulation results; the viscosity of the liquid phase and the temperature of the domain are depicted on the left and right side of the plots, respectively.

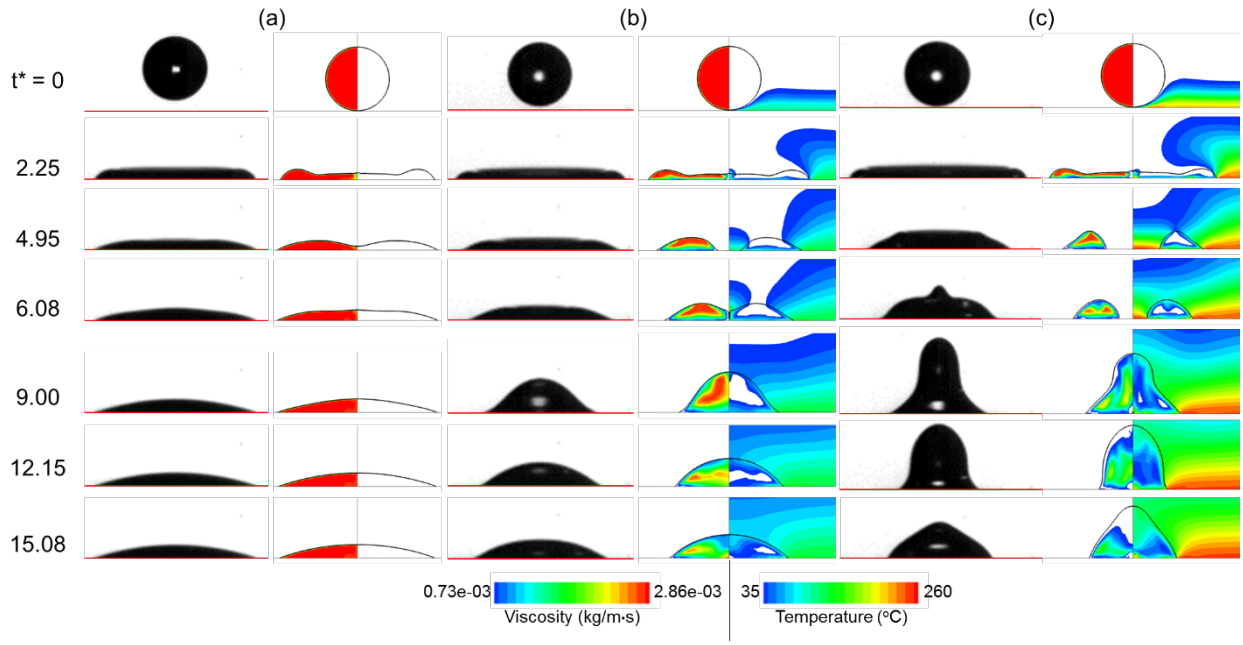

Figure 8: Sequential images (experiment and simulation) of Diesel fuel droplet impact on a heated aluminium surface for We=65 and P=1 bar: (a) T_w=25°C, (b) T_W=140°C and (c) T_W=260°C. For the simulation results, values of viscosity and temperature below the lower contour level are cut-off.

After impact, the droplet initially spreads on the surface with nearly the same spreading velocity for all cases (t*=2.25). After reaching its maximum spreading, for impact at T_W=140°C and 260°C the droplet begins to retract (t*=4.95) towards its centre until reaching a minimum shrinking position without rebounding from the surface (t*=9 and 12.15 for T_W=140°C and 260°C). Depending on the surface temperature, the droplet oscillates on the surface until it reaches its final shape. In contrast, at surface temperature of T_W=25°C nearly no recoiling was observed and the droplet shape was not changed after the maximum spreading diameter. This can be seen in Figure 8a for t*>2.25. Numerical results indicate that as the temperature of the surface increases, the change in viscosity is more profound, as the droplet heats up quicker. This is the main reason for the quicker recoiling of the drop as the surface temperature increases.

Figure 9 depicts the temporal evolution of apparent dynamic contact angle and spreading factor β= (D (t)/D_0) for three different surface temperatures keeping a constant We=65. The time to reach the maximum spreading was slightly decreased by increasing the surface temperature. The droplet spreads with the same velocity approximately until t*=1, as the kinetic energy is the dominant factor in the initial spreading. By increasing the surface temperature, the droplet undergoes through stronger retraction and the maximum receding diameter decreases. The spreading factor at the end of this oscillation decreases with increasing wall temperature. A drastic decrease in dynamic contact angle is observed until t*=6 in a nearly similar manner for all surface temperatures. This shows that the decreasing dynamic contact angle during the initial phase is mainly related to the inertia of the radially spreading liquid [78]. However, during the recoiling phase, the values of the dynamic contact angle after t*=6 are significantly different for the three values of wall temperature tested. The dynamic contact angle for lower surface temperature is almost constant, while it increases significantly with increasing surface temperature. The numerical results are in good agreement with the experimental measurements for the prediction of spreading diameter, maximum value and temporal evolution, as well as the droplet oscillating behaviour and the quicker recoiling phase for higher surface temperatures. The equilibrium position that the droplet rests at the end of the impingement is not the same, between experiments and simulation (simulation radius is smaller), as for small contact angle values, the grid resolution should be significantly increased to capture the prescribed angle value.

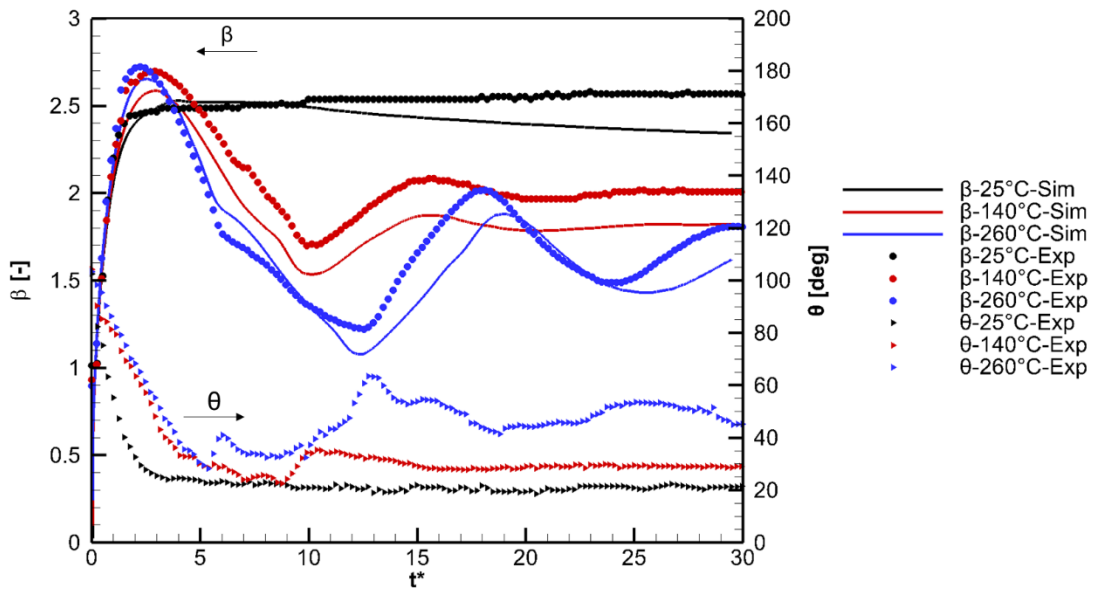

Figure 9: Effect of surface temperature on time evolution of dynamic contact angle and spreading factor for We=65 and 1 bar chamber pressure at T_W=25, 140, 260°C

In Figure 10, the predicted viscosity of the liquid phase as the droplet spreads on the surface is presented at three different time instances for three different surface temperatures. It is clear that viscosity values are lower on the liquid-solid interface as the temperature of the surface increases; this is due to the increased heat transfer rate between the solid and the liquid. This viscosity decrease results to reduced kinetic energy dissipation and thus, faster recoiling behaviour. The difference in recoiling behaviour has already been observed in the experimental works of [26], [79], [80], where it is mentioned that the increased liquid viscosity at hydrophilic surfaces and low surface temperatures increases the viscous dissipation, which in turn reduce the available energy for retraction. Surface tension coefficient also decreases with temperature, but the effect of viscosity is more significant. This is why the droplet forms a higher contact angle with the solid surface, a phenomenon that is captured by the simulation.

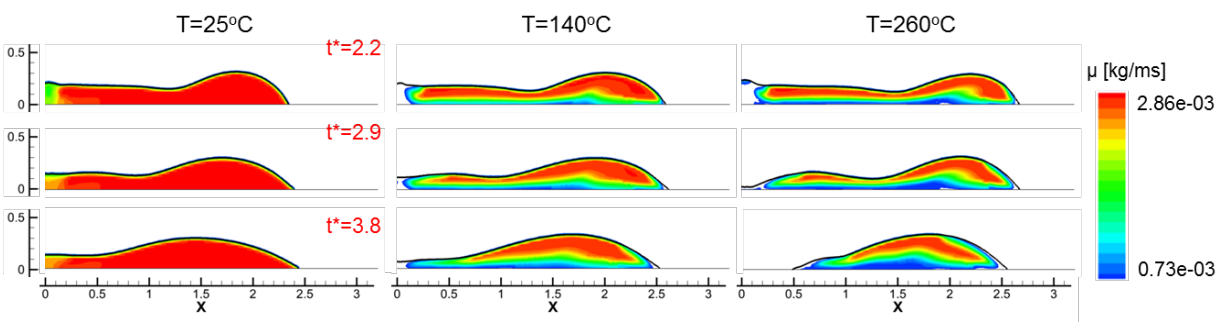

Figure 10: Droplet rim motion at 3 time instances (hysteresis and recoil) for 3 different surface temperatures of T_W=25, 140, 260°C, We=65 and 1 bar chamber pressure.

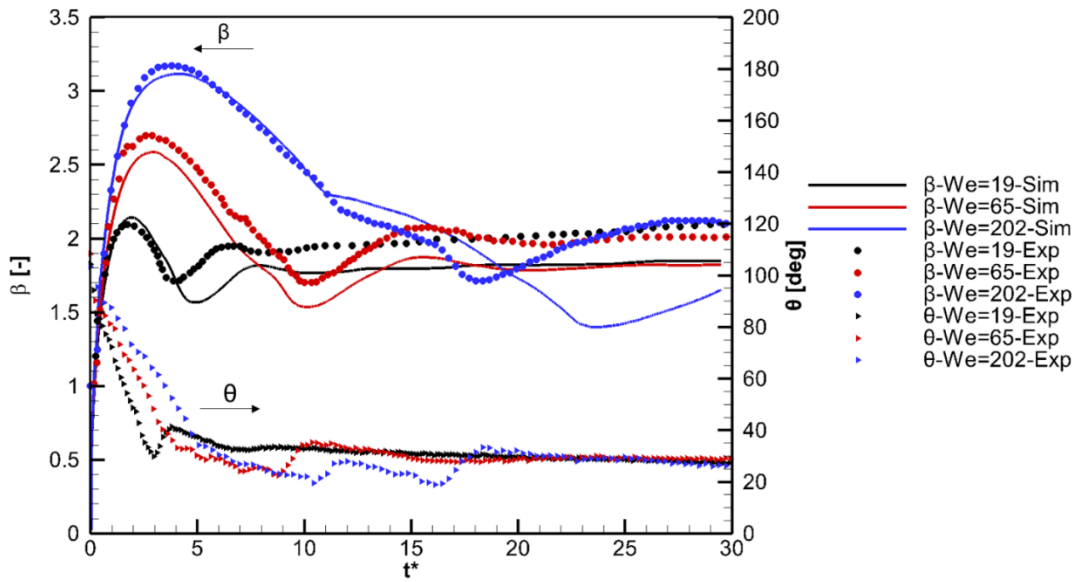

Figure 11: Effect of impact Weber number on time evolution of dynamic contact angle and spreading factor at surface temperature of T_W=140°C and 1 bar chamber pressure for We=19, 65 and 202

Figure 12a shows the combined effect of ambient air pressure, impact Weber number and surface temperature on the temporal evolution of the dynamic contact angle and spreading factor for We=19 and 65. The oscillation frequency and amplitude seems to be only dependent on the surface temperature. The effect of the air pressure is quite insignificant for these conditions, as also reported in [81]. However, a weak suppression of the droplet spreading at P=2bar is observed, since the spreading factor β obtains a lower value compared to P=1bar test case. This can be attributed to the increased aerodynamic drag effect at the triple contact point, as the density of the ambient air is double at 2 bar chamber pressure compared to atmospheric condition; this is also reproduced by the numerical results in [5], showing that increasing the value of the ambient pressure reduces the maximum air velocity in the vicinity of the contact area.

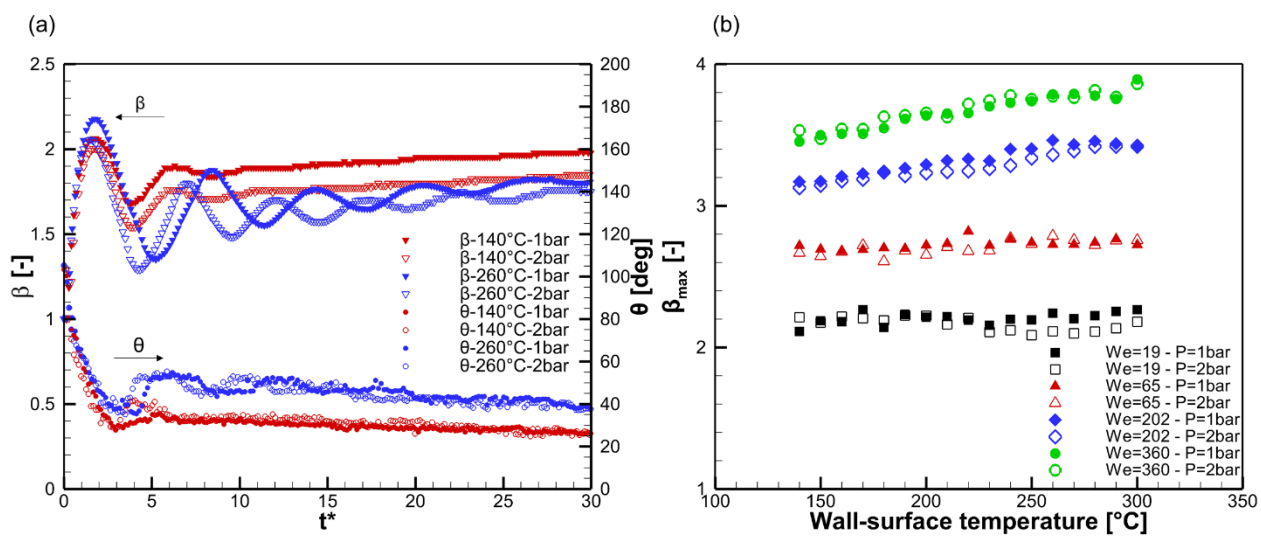

Figure 12: (a) Temporal variation of the dynamic contact angle θ and spreading factor β for We=19 at T_W=140 and 260°C at P=1 and 2bar (b) Effect of surface temperature, impact Weber number and ambient air pressure on maximum spreading diameter

The maximum spreading factor is an important parameter for characterising the heat transfer, as the contact area designates the overall heat transfer between the heated surface and the droplet. Figure 12b shows the maximum spreading (normalised with the droplet diameter), for different values of We and surface temperature in the range of

140°C<T_W<300°C at 1 and 2 bar chamber pressure. It is clear that for We<65, the maximum spreading factor does not vary significantly with increasing surface temperature. For higher values of the Weber number, there is a slight increase of the maximum spreading factor with surface temperature. On the contrary, the impact Weber number has a significant influence on the maximum spreading diameter, as increase of its value from 19 to 360 leads to a subsequent, almost double increase of the maximum spreading factor. This shows that the initial stage of the impact until the maximum spreading diameter is affected primarily by impact kinetic energy rather than thermal effects.

4 Conclusions

Thermal induced effects are fairly different between multi- and single component liquids. In this study, new experimental data for the impact of standard Diesel fuel droplets on a heated surface within a gaseous (air) environment at 1 and 2 bar pressure has been investigated for a wide range of Weber number and surface temperature values, employing both high speed visualization and CFD simulations. The six distinct impact regimes observed have been indicated on the We-T map for all conditions tested; these are termed as stick, partial-rebound, breakup, breakup-rebound, splash and rebound. Critical (We, T) value pairs have been identified, which signify the transition to breakup, splash and rebound regimes. At 1 bar air pressure, splash occurs for We>490 regardless of the wall-surface temperature value. The rebound regime transition to which, in essence, indicates that Leidenfrost condition, was observed for T_W≥340°C. The breakup regime was observed for We≥350 and 270°C≤T≤T_L. By increasing the ambient air pressure to 2 bars, the critical We number for splash was reduced to 350 and the Leidenfrost-point temperatures of rebound and breakup-rebound regimes were increased by 20°C and 30°C, respectively. In addition, the transition line of breakup regime was shifted by nearly 70°C.

The effect of wall-surface temperature and impact Weber number on wetting parameters (spreading factor and dynamic contact angle) have been numerically and experimentally assessed. Numerical and experimental results were found to be in a good agreement in terms of droplet shapes, spreading behaviour, and oscillation frequency of the droplet interface. It has also been confirmed that by increasing wall-surface temperature, the droplet exhibits a strongly oscillating behaviour during the expansion and recoil phases, due to a reduction of liquid viscosity at higher surface temperature. This stronger recoiling behaviour also increases the value of the dynamic contact angle with the solid surface. In addition, an increase in the Weber number results in a larger value of the spreading factor while the oscillating frequency and final droplet shape remain unchanged.

To the best of authors' knowledge, this the first attempt to classify the impact outcome of a complex hydrocarbon fuel droplet on a flat heated surface. Comparisons with the available experimental data for the single component fluids clearly shows significant differences, especially in terms of transition to Leidenfrost and breakup regimes; differences in liquid composition and non-homogeneity of the Diesel fuel droplet at the temperature above any of its component's boiling temperature, results in different flow process and evaporating behaviour during the impact, and consequently the final outcome. Breakup transition has been also captured by CFD simulations, with good agreement with the experimental data.

5 Acknowledgments

The authors would like to acknowledge the contribution of The Lloyd's Register Foundation. Lloyd's Register Foundation helps to protect life and property by supporting engineering-related education, public engagement and the application of research.

6 Data accessibility.

The datasets supporting this article have been uploaded as part of the electronic supplementary material.

7 Competing interests.

We have no competing interests

8 Authors' contributions.

HJ conducted the experimental investigation as part of his PhD. IM performed the numerical simulations, as part of his PhD. MG is the project PI and 1st supervisor of the 2 PhD students; NM is the Co-investigator and 2nd supervisor. IK is

the post-doctoral researcher who assisted in the analysis of the experimental data. All authors gave final approval for publication.

9 Funding statement.

The research was financially supported partially by The Lloyd's Register Foundation and City, University of London supporting the studentship of HJ.

10 Nomenclature

We	Weber number ($\rho V_0^2 D_0/\sigma$)	T	Surface temperature [°C]
Re	Reynolds number ($\rho V_0 D_0/\mu$)	P	Ambient pressure [bar]
Oh	Ohnesorge ($\sqrt{We}/Re$)	T_W	Wall-surface temperature
ρ	Density [kg/m^3]	T_{BP}	Liquid boiling temperature
σ	Surface tension [N/m]	T_L	Leidenfrost temperature
V_0	Impact velocity [m/s]	T*	Ratio of wall-surface superheat (T_W/T_{BP})
D_0	Droplet diameter at impact time [m]	K	Thermal conductivity [W/m.K]
t*	Dimensionless time ($t \times V_0/D_0$)	C	Specific heat capacity [J/kg.K]

11 References

[1] S. Yao and K. Cai, "The dynamics and Leidenfrost temperature of drops impacting on a hot surface at small angles," *Exp. Therm. Fluid Sci.*, 1988.

[2] R. Rioboo, C. Tropea, and M. Marengo, "Outcomes from a drop impact on solid surfaces," *At. Sprays*, 2001.

[3] Š. Šikalo, C. Tropea, and E. Ganić, "Dynamic wetting angle of a spreading droplet," *Exp. Therm. Fluid Sci.*, 2005.

[4] M. Shirota, M. van Limbeek, C. Sun, and A. Prosperetti, "Dynamic Leidenfrost effect: relevant time and length scales," *Phys. Rev.*, 2016.

[5] J. Liu, H. Vu, S. Yoon, and R. Jepsen, "Splashing phenomena during liquid droplet impact," *At.*, 2010.

[6] A. Moreira, A. Moita, and M. Panao, "Advances and challenges in explaining fuel spray impingement: How much of single droplet impact research is useful?," *Prog. energy Combust.*, 2010.

[7] A. Yarin, "Drop impact dynamics: splashing, spreading, receding, bouncing," *Annu. Rev. Fluid Mech.*, 2006.

[8] C. Tang, J. Zhao, P. Zhang, and C. Law, "Dynamics of internal jets in the merging of two droplets of unequal sizes," *J. Fluid Mech.*, 2016.

[9] V. Bertola, "An impact regime map for water drops impacting on heated surfaces," *Int. J. Heat Mass Transf.*, 2015.

[10] G. Liang, S. Shen, Y. Guo, and J. Zhang, "Boiling from liquid drops impact on a heated wall," *Int. J. Heat Mass*, 2016.

[11] J. G. Leidenfrost, "On the fixation of water in diverse fire," *Int. J. Heat Mass Transf.*, vol. 9, no. 11, pp. 1153–1166, Nov. 1966.

[12] G. Liang, X. Mu, Y. Guo, S. Shen, S. Quan, and J. Zhang, "Contact vaporization of an impacting drop on heated surfaces," *Exp. Therm. Fluid Sci.*, 2015.

[13] J. Burton, A. Sharpe, R. van der Veen, and A. Franco, "Geometry of the vapor layer under a Leidenfrost drop," *Phys. Rev.*, 2012.

[14] M. Khavari, C. Sun, D. Lohse, and T. Tran, "Fingering patterns during droplet impact on heated surfaces," *Soft Matter*, 2015.

[15] S. Nishio and M. Hirata, "Direct contact phenomenon between a liquid droplet and high temperature solid surface," *Sixth Int. Heat Transf.*, 1978.

[16] G. Celata, M. Cumo, A. Mariani, and G. Zummo, "Visualization of the impact of water drops on a hot surface: effect of drop velocity and surface inclination," *Heat mass Transf.*, 2006.

[17] J. BERNARDIN, C. Stebbins, and I. Mudawar, "Effects of surface roughness on water droplet impact history and heat transfer regimes," *Int. J. Heat*, 1996.

[18] I. Buchmüller, "Influence of pressure on Leidenfrost effect," *PhD Thesis*, 2014.

[19] M. Marengo, C. Antonini, and I. Roisman, "Drop collisions with simple and complex surfaces," *Curr. Opin. Colloid*, 2011.

[20] I. V. Roisman, L. Opfer, C. Tropea, M. Raessi, J. Mostaghimi, and S. Chandra, "Drop impact onto a dry surface: Role of the dynamic contact angle," *Colloids Surfaces A Physicochem. Eng. Asp.*, vol. 322, no. 1, pp. 183–191, 2008.

[21] K. Yokoi, D. Vadillo, and J. Hinch, "Numerical studies of the influence of the dynamic contact angle on a droplet impacting on a dry surface," *Phys. Fluids (1994-*, 2009.

[22] I. Roisman, L. Opfer, C. Tropea, and M. Raessi, "Drop impact onto a dry surface: role of the dynamic contact

angle," *Colloids Surfaces A*, 2008.
[23] W. M. Healy, J. G. Hartley, and S. I. Abdel-Khalik, "On the Validity of the Adiabatic Spreading Assumption in Droplet Impact Cooling," *Repr. from Int. J. Heat Mass Transf.*, vol. 44, pp. 3869–3881, 2001.
[24] S. Kandlikar and M. Steinke, "Contact angles and interface behavior during rapid evaporation of liquid on a heated surface," *Int. J. Heat Mass Transf.*, 2002.
[25] S. Chandra and C. T. Avedisian, "On the Collision of a Droplet with a Solid Surface," *Proc. R. Soc. A Math. Phys. Eng. Sci.*, vol. 432, no. 1884, pp. 13–41, Jan. 1991.
[26] A. Alizadeh, V. Bahadur, S. Zhong, and W. Shang, "Temperature dependent droplet impact dynamics on flat and textured surfaces," *Appl. Phys.*, 2012.
[27] H. Fujimoto, Y. Oku, T. Ogihara, and H. Takuda, "Hydrodynamics and boiling phenomena of water droplets impinging on hot solid," *Int. J.*, 2010.
[28] E. Negeed, S. Hidaka, M. Kohno, and Y. Takata, "High speed camera investigation of the impingement of single water droplets on oxidized high temperature surfaces," *Int. J.*, 2013.
[29] M. Driscoll and S. Nagel, "Ultrafast interference imaging of air in splashing dynamics," *Phys. Rev. Lett.*, 2011.
[30] G. E. Cossali, M. Marengo, and M. Santini, "Secondary atomisation produced by single drop vertical impacts onto heated surfaces," *Exp. Therm. Fluid Sci.*, vol. 29, no. 8, pp. 937–946, 2005.
[31] S. Jung and I. Hutchings, "The impact and spreading of a small liquid drop on a non-porous substrate over an extended time scale," *Soft Matter*, 2012.
[32] G. Liang, Y. Guo, Y. Yang, S. Guo, and S. Shen, "Special phenomena from a single liquid drop impact on wetted cylindrical surfaces," 2013.
[33] T. Gilet and J. Bush, "Droplets bouncing on a wet, inclined surface," *Phys. Fluids*, 2012.
[34] C. Stevens, "Scaling of the splash threshold for low-viscosity fluids," *EPL (Europhysics Lett.*, 2014.
[35] R. Rioboo, M. Marengo, and C. Tropea, "Time evolution of liquid drop impact onto solid, dry surfaces," *Exp. Fluids*, 2002.
[36] V. Bertola, "Dynamic wetting of dilute polymer solutions: the case of impacting droplets," *Adv. Colloid Interface Sci.*, 2013.
[37] H. Fujimoto, S. Watanabe, T. Okamoto, and T. Hama, "Photographic study of hydrodynamics of drops of aqueous polymer solution impinging on hot solid," 2015.
[38] E. Kompinsky, G. Dolan, and E. Sher, "Experimental study on the dynamics of binary fuel droplet impacts on a heated surface," *Chem. Eng. Sci.*, 2013.
[39] A. Moita and A. Moreira, "Development of empirical correlations to predict the secondary droplet size of impacting droplets onto heated surfaces," *Exp. Fluids*, 2009.
[40] A. Moita and A. Moreira, "The deformation of single droplets impacting onto a flat surface," 2002.
[41] S. Herbert, S. Fischer, and T. Gambaryan-Roisman, "Local heat transfer and phase change phenomena during single drop impingement on a hot surface," *Int. J. Heat Mass Transf.*, 2013.
[42] H. Nair, H. Staat, T. Tran, A. van Houselt, and A. Prosperetti, "The Leidenfrost temperature increase for impacting droplets on carbon-nanofiber surfaces," *Soft Matter*, 2014.
[43] J. Moon, D. Kim, and S. Lee, "Spreading and receding characteristics of a non-Newtonian droplet impinging on a heated surface," *Exp. Therm. Fluid Sci.*, 2014.
[44] D. Segawa, T. Kadota, S. Nakaya, and K. Takemura, "A liquid film or droplet of miscible binary fuel burning on a heated surface at elevated pressures," *Proc. Combust. Inst.*, 2009.
[45] A. Mahulkar, G. Marin, and G. Heynderickx, "Droplet–wall interaction upon impingement of heavy hydrocarbon droplets on a heated wall," *Chem. Eng. Sci.*, 2015.
[46] A. Trujillo-Pino, K. Krissian, M. Alemán-Flores, and D. Santana-Cedrés, "Accurate subpixel edge location based on partial area effect," *Image Vis. Comput.*, vol. 31, no. 1, pp. 72–90, Jan. 2013.
[47] Š. Šikalo, M. Marengo, C. Tropea, and E. Ganić, "Analysis of impact of droplets on horizontal surfaces," *Exp. Therm. fluid*, 2002.
[48] I. Malgarinos, N. Nikolopoulos, and M. Marengo, "VOF simulations of the contact angle dynamics during the drop spreading: standard models and a new wetting force model," *Adv. colloid and, 2014*.
[49] I. Malgarinos, N. Nikolopoulos, and M. Gavaises, "Numerical investigation of heavy fuel droplet-particle collisions in the injection zone of a Fluid Catalytic Cracking reactor, Part I: Numerical model and 2D simulations," *Fuel Process. Technol.*, vol. 156, pp. 317–330, 2017.
[50] I. Malgarinos, N. Nikolopoulos, and M. Gavaises, "A numerical study on droplet-particle collision dynamics," *Int. J. Heat Fluid Flow*, vol. 61, pp. 499–509, 2016.
[51] X. Ma, F. Zhang, K. Han, B. Yang, and G. Song, "Evaporation characteristics of acetone–butanol–ethanol and diesel blends droplets at high ambient temperatures," *Fuel*, vol. 160, pp. 43–49, Nov. 2015.
[52] K. Han, B. Yang, C. Zhao, G. Fu, X. Ma, and G. Song, "Experimental study on evaporation characteristics of ethanol–diesel blend fuel droplet," *Exp. Therm. Fluid Sci.*, vol. 70, pp. 381–388, Jan. 2016.
[53] G. Strotos, G. Aleksis, M. Gavaises, K.-S. Nikas, N. Nikolopoulos, and A. Theodorakakos, "Non-dimensionalisation parameters for predicting the cooling effectiveness of droplets impinging on moderate temperature solid surfaces," *Int. J. Therm. Sci.*, vol. 50, no. 5, pp. 698–711, 2011.
[54] L. Villegas, S. Tanguy, G. Castanet, and O. Caballina, "Direct numerical simulation of the impact of a droplet

onto a hot surface above the Leidenfrost temperature," *Int. J.*, 2017.
[55] N. Kolev, "Multiphase Flow Dynamics 3: Turbulence, Gas Absorption and Release, Diesel Fuel Properties. 2002," *Springer Verlag Berlin Heidelberg*.
[56] N. I. Kolev, "Thermodynamic and transport properties of diesel fuel," in *Multiphase Flow Dynamics 3*, Berlin, Heidelberg: Springer Berlin Heidelberg, pp. 269–302.
[57] C. L. Yaws, *Yaws' handbook of thermodynamic and physical properties of chemical compounds : physical, thermodynamic and transport properties for 5,000 organic chemical compounds*. Norwich, N.Y. : Knovel, 2003.
[58] R. Lin and L. L. Tavlarides, "Thermophysical properties needed for the development of the supercritical diesel combustion technology: Evaluation of diesel fuel surrogate models," *J. Supercrit. Fluids*, vol. 71, pp. 136–146, Nov. 2012.
[59] A. Moreira, A. Moita, E. Cossali, and M. Marengo, "Secondary atomization of water and isooctane drops impinging on tilted heated surfaces," *Exp.*, 2007.
[60] H. J. J. Staat *et al.*, "Phase diagram for droplet impact on superheated surfaces," *J. Fluid Mech.Phys. Rev. Lett. J. Fluid Mech*, vol. 779, no. 772, pp. 630–648, 2015.
[61] C. Clavijo, J. Crockett, and D. Maynes, "Hydrodynamics of droplet impingement on hot surfaces of varying wettability," *Int. J. Heat Mass*, 2017.
[62] T. Tran, H. Staat, A. Prosperetti, C. Sun, and D. Lohse, "Drop impact on superheated surfaces," *Phys. Rev. Lett.*, 2012.
[63] J. Bernardin, C. Stebbins, and I. Mudawar, "Mapping of impact and heat transfer regimes of water drops impinging on a polished surface," *J. Heat Mass Transf.*, 1997.
[64] T. Xiong and M. Yuen, "Evaporation of a liquid droplet on a hot plate," *Int. J. Heat Mass Transf.*, 1991.
[65] K. Baumeister, R. Henry, and F. Simon, "Role of the Surface in the Measurement of the Leidenfrost Temperature," 1970.
[66] V. Borishansky, "Heat transfer to a liquid freely flowing over a surface heated to a temperature above the boiling point," *Probl. heat Transf. Dur. a Chang. state (ed.*, 1953.
[67] H. Blaszkowska-Zakrzewska, "Rate of Evaporation of Liquids from a Heated Metallic Surface," *Bull. Int. VAcademie Pol.*, 1930.
[68] L. H. J. Wachters and N. A. J. Westerling, "The heat transfer from a hot wall to impinging water drops in the spheroidal state," *Chem. Eng. Sci.*, vol. 21, no. 11, pp. 1047–1056, 1966.
[69] R. Chen, M. Lu, V. Srinivasan, Z. Wang, and H. Cho, "Nanowires for enhanced boiling heat transfer," *Nano*, 2009.
[70] W. Zhang, T. Yu, J. Fan, W. Sun, and Z. Cao, "Droplet impact behavior on heated micro-patterned surfaces," *J. Appl. Phys.*, 2016.
[71] T. Tran, H. Staat, A. Susarrey-Arce, and T. Foertsch, "Droplet impact on superheated micro-structured surfaces," *Soft Matter*, 2013.
[72] A. Wang, C. Lin, and C. Cheng, "Pattern analysis of a single droplet impinging onto a heated plate," *Heat Transf. Res.*, 2005.
[73] P. H. Z Levin, "Levin, Z. and Hobbs, P. V., Charge separation due... - Google Scholar," *Am. Meteorol. Soc.*, vol. 51, pp. 577–586, 1970.
[74] L. Xu, W. Zhang, and S. Nagel, "Drop splashing on a dry smooth surface," *Phys. Rev. Lett.*, 2005.
[75] M. Bussmann, S. Chandra, and J. Mostaghimi, "Modeling the splash of a droplet impacting a solid surface," *Phys. Fluids*, vol. 12, no. 12, pp. 3121–3132, Dec. 2000.
[76] K. Yokoi, "A practical numerical framework for free surface flows based on CLSVOF method, multi-moment methods and density-scaled CSF model: Numerical simulations of," *J. Comput. Phys.*, 2013.
[77] Y. Guo, Y. Lian, and M. Sussman, "Investigation of drop impact on dry and wet surfaces with consideration of surrounding air," *Phys. Fluids*, vol. 28, no. 7, p. 73303, Jul. 2016.
[78] J. Lee and S. Lee, "Dynamic wetting and spreading characteristics of a liquid droplet impinging on hydrophobic textured surfaces," *Langmuir*, 2011.
[79] J. H. Moon, M. Cho, and S. H. Lee, "Dynamic wetting and heat transfer characteristics of a liquid droplet impinging on heated textured surfaces," *Int. J. Heat Mass Transf.*, vol. 97, pp. 308–317, 2016.
[80] J. H. J. Moon, D. Y. D. Kim, and S. S. H. Lee, "Spreading and receding characteristics of a non-Newtonian droplet impinging on a heated surface," *Exp. Therm. FLUID Sci.*, vol. 57, pp. 94–101, 2014.
[81] N. N. K. Mishra, Y. Zhang, and A. Ratner, "Effect of chamber pressure on spreading and splashing of liquid drops upon impact on a dry smooth stationary surface," *Exp. Fluids*, vol. 51, no. 2, pp. 483–491, 2011.